A novel approach for wettability estimation in geological systems by fluid-solid interfacial area measurement using tracers

Deepshikha Singh[a], Shantanu Roy[a], Harish Jagat Pant[b], Jyoti Phirani[c*]

[a] *Department of Chemical Engineering, Indian Institute of Technology Delhi, Hauz Khas, New Delhi, India*

[b] *Isotope and Radiation Application Division, Bhabha Atomic Research Centre, Trombay, Mumbai, India*

[c] *Department of Civil and Environmental Engineering, University of Strathclyde, Glasgow, United Kingdom*

Abstract

Wettability plays a vital role in many applications of flow in porous media and affects Darcy scale flow parameters by influencing the fluid-solid interfacial area. Therefore, quantifying the fluid-solid interfacial area can provide a way to measure wettability at the Darcy scale. Here, we experimentally explore a dual-tracer method, which can also be scaled to large geological reservoirs to quantify the fluid-solid interfacial area during the multiphase flow through a porous medium for different wetting conditions. Using our experiments, we demonstrate the influence of different saturations, wettability and flow conditions on the solid-liquid interfacial area. When oil is in the residual phase, we observe that the solid-water interfacial area increases with the increase in water saturation for the water-wet and mixed-wet cases. However, the water-solid interfacial area decreases with an increase in water saturation for

the oil-wet case. We increase the water saturation by increasing the water flow rate; therefore, the anomalous behaviour seen in the oil-wet case can be attributed to the rearrangement of oil and water at higher water flow rates. When both oil and water are flowing, the solid-water interfacial area increases with water saturation for all the wettability cases and increases in water wettability as anticipated.

Keywords: Two-tracer method; Wettability alteration; solid-liquid interfacial area; Enhanced oil recovery.

Synopsis: Wettability measurements at Darcy-scale give a broad idea of overall subsurface wetting conditions for application in CO_2 sequestration, ground-water remediation or oil recovery.

1. Introduction

Wettability is one of the rock's constitutive properties that define a solid surface's preference to contact one liquid over another. Wettability controls the location [1], distribution [2, 3], and the characteristics of the fluid flow [4, 5] by controlling the capillary pressure [6] during multiphase flow in a porous medium. Wettability and wettability alteration play a vital role in paper microfluidic devices [7], oil recovery from reservoirs [8], particle coating [9], printing [10], catalyst behaviour in packed bed reactors [11], textile industry [12], and membrane distillation [13]. Depending on the application, hydrophobic or hydrophilic surface is preferred. Therefore, quantifying the wettability and wettability alteration of a porous medium is essential.

Various wettability quantification techniques have been explained at different scales [14] for a porous medium, where the majority of the medium is inaccessible for visualization. In particular, rock's wettability in the geological reservoirs, especially for oil reservoirs, has been described by many researchers [15, 16, 17, 18]. Anderson et al. [19] has explained in detail the concepts of wettability and reviewed the three most commonly used quantitative methods: Contact Angle method, Amott-Harvey Index method, United States Bureau of Mines (USBM) method with their limitations and applications. However, many qualitative ways such as; the shape of the permeability curves, imbibition rates, capillary pressure saturation curve, and displacement capillary pressure in a porous medium, and flotation of the solid powder on the liquid distinguish the wetting state of a solid [20, 21, 22, 23, 24]. The wettability quantification of a porous medium at the Darcy-scale is still elusive due to the pore space's irregular morphology and topology leading to non-universality of the porous media characterization [25, 26, 27, 28, 29]. Recently, four Minkowski functionals, i.e., curvature, volume, topology (Euler characteristic) of the fluid phases and the pore surface area and pore structure, have been targeted for a universal method of characterizing multiphase flow in porous medium [30, 31, 32]. The fluid-fluid and fluid-solid interfacial area, which are the geometric state variables in the multiphase flow, are being explored for quantifying wettability [12, 33, 34, 35, 36]. To that end, X-ray micro-tomography has been frequently used to capture the

contact angle of the two immiscible fluids [37, 38, 39, 40] and the fluid-solid contact area [41] in a porous medium. However, applying the X-ray micro-CT and electron microscopy method at large scale such as in a geological reservoir is challenging due to the high-resolution requirements of the images [42, 43, 44, 45, 46, 47], and inaccessibility of the reservoirs.

For geological reservoir, nuclear Magnetic Resonance (NMR) [48, 49, 50], and 3D magnetic resonance imaging (MRI) [51] have been explored for quantify wettability. However, the NMR-based approach can only be applied in the area adjacent to the well of the light-oil reservoirs [52]. A method of quantifying the aggregate, large-scale wettability during flow in a porous medium is still needed.

Tracers have been extensively used to characterize the large-scale porous medium in flowing conditions [25, 53, 54, 55, 56, 57, 58] for fraction of the fluids present or heterogeneity. More recently, interfacial partitioning tracer test (IPTT) has been used to examine the influence of fluid saturation, pore texture, and fluid-displacement regimes on the fluid-fluid interface inside the porous medium [28, 59, 60, 61, 62, 63, 64, 65, 66, 67, 68, 69, 70]. The estimated fluid-fluid interfacial area [68] is indirectly related to the rock's wettability. Recently, fluid-solid interfacial area and saturation relationships have been proposed as an indicator of the wettability of porous media during the multiphase flow in multiple studies [71, 72, 73]. However, so far,

the possibility of determining these relationships remains limited due to the pore-scale image analysis and the requirement of a very high-resolution limit to characterize wettability. Based on X-ray micro tomography work by Garfi et al. [34, 74], if we can directly quantify the fluid-solid interfacial area, then we can use it to differentiate the wetting state of the geological reservoir. In the present work we use tracers to determine the fluid-solid interfacial area at darcy scale. Using the present work, we hope to find a link between the pore scale wettability found using images and darcy scale wettability.

Singh et al. [75] made the first step to use a two-tracer method, which they successfully implemented in a lab scale porous medium, to quantify fluid-solid interfacial area at a given wetting condition and when one phase is at the residual saturation. They showed that the wetting phase has more contact area with the porous solid at a given residual saturation in comparison to the non-wetting phase.

In this work, we use the two-tracer method to quantify the fluid-solid interfacial area at different wetting and flow conditions. The general workflow presented in this paper is depicted in Figure 1. We focus on water-solid interface area at water-wet, oil-wet, and mixture of 50% water-wet and 50% oil-wet glass beads i.e., mixed-wet conditions. We do experiments when oil is in the residual phase and only water is moving and when oil and water both are moving. When oil is the residual phase, we increase the injection

rate of water to increase water saturation and find that solid-water interfacial area increases with water saturation for the water-wet and mixed-wet cases. However, for the oil-wet case, the water-solid interfacial area decreases with increase in water saturation. This can be attributed to the rearrangement of the water and oil phases in the porous medium due to increase in flow rate [76]. When both phases are flowing, then the water-solid interfacial area increases monotonically with water saturation and water wettability as expected.

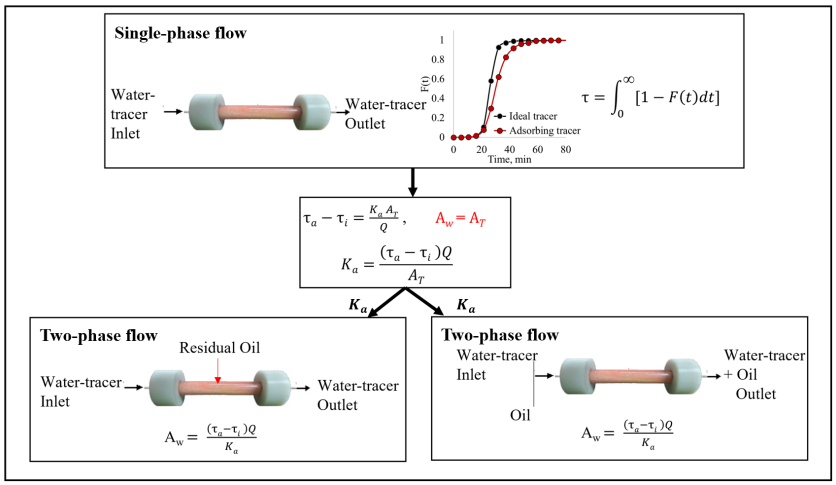

Figure 1: The workflow for measuring the solid-liquid interfacial area during a multiphase flow system in a porous medium using the dual-tracer method, which is proposed in this paper. Here, τ (min) is the mean residence time calculated using measured cumulative exit age density function $F(t)$. τ_i (min) and τ_a (min) are the mean residence times of the ideal and adsorbing tracers, respectively. Q (ml/min) is the liquid flow rate, K_a (ml/g) is the adsorption partition coefficient onto the solid matrix, A_T (g) is the total mass of the glass beads in contact with the porous medium and A_w (g) is the mass of the glass beads in contact with water during two-phase flow which is directly proportional to the interfacial area of the glass beads and water for a given specific surface area of the glass beads.

2. Materials

We use glass beads of sizes $150 - 200$ (μm) to create a proxy laboratory-scale one-dimensional cylindrical reservoir [77]. We use n-dodecane (DD) as an organic phase, and Milli-Q purified Deionized Water (DIW) as an aqueous phase. Figure 2 shows the experimental setup where we use the syringe pumps to inject the fluids in the cylindrical porous medium made of glass beads. The tracer is used only for the aqueous phase for which we use Fluorescein Sodium Salt (FSS) as an ideal tracer and Sodium Thiosulfate (STS) [78] as an adsorbing tracer. We used red organic dye to colour the organic phase for better visualisation. In Table 1, we list the materials and their properties used in this work. We use hydrochloric acid, methanol, toluene and trichloromethyl silanes to treat the glass beads. We obtained all the chemicals from Sigma-Aldrich Chemicals Pvt. Ltd., India.

Table 1: List of chemicals and their properties.

Chemical (Formula)	Mol.Wt., $(\frac{g}{mol})$	Density, $(\frac{g}{cc})$	Appearance
n-dodecane ($C_{12}H_{26}$)	170.34	0.75	Colorless liquid
Oil Red O ($C_{26}H_{24}N_4O$)	408.49	0.84	Red powder
Fluorescein Sodium Salt ($C_{20}H_{10}Na_2O_5$)	376.28	1.60	Dark red powder
Sodium Thiosulfate ($Na_2S_2O_3.5H_2O$)	248.18	1.67	White crystals
Hydrochloric Acid (HCl) (0.01 M aqueous solution)	36.46	1.00	Colorless liquid
Methanol (CH_3OH)	32.04	0.79	Colorless liquid
Toluene (C_7H_8)	92.14	0.87	Colorless liquid
Trichloromethyl silane (CH_3Cl_3Si)	149.47	1.27	Colorless liquid

Figure 2: The step-input tracer flow experimental setup.

2.1. Preparation of the glass beads

We perform the flow experiments at different wetting conditions; therefore, we prepare water-wet and oil-wet glass beads. First, to prepare the water-wet surface of the glass beads, we clean the glass beads using 0.1 M HCl solution. Then, we wash the glass beads with distilled water to remove any residue and dry the glass beads in an oven at 80^0C till they are completely dry. The glass beads are now water-wet [79].

We now use the silanization process to alter the water-wet glass beads to oil-wet [80, 81]. We prepare 1-4% diluted solutions of 3-Chloro Methyl Silane (TCMS) in dehydrated toluene. We soak the water-wet glass beads prepared above in the diluted solutions of the silane for 30 minutes. A thin film of methylpolysiloxanes immediately coats the glass bead. TCMS has three hydrolyzable groups that produce extensive cross-linking, making a three-dimensional silane multilayer on the silica surface a more stable coating than

a monolayer. Anhydrous hydrochloric acid also forms during this reaction [79]. We rinse the glass beads with methanol and thoroughly dry them at 50^0C in the oven, favouring the cross-linking reaction of the silane on the glass beads altering their wettability. We confirm the wettability alteration of the glass beads using the flotation technique [82] as described below in Section (2.2).

2.2. Flotation test for qualitative wettability characterization

We perform the flotation test in a 5 *ml* acrylic test tube. We fill five tubes with 3 *ml* water and slowly pour 1 *g* glass beads over the water, which we prepared using different concentrations of TCMS. Figure 3 demonstrates the flotation test result at various times that qualitatively compare the wettability of the treated glass beads. Figure 3(a) shows the initial ($t = 0$) stage of the flotation test where tube 1 has water-wet glass beads completely submerged in the water. The remaining tubes have glass beads treated with various concentrations of TCMS in dehydrated toluene. Initially, the silane treated glass beads are floating at the top of the water as shown in Figure 3(a). After one hour, the glass beads treated with 4% silane and 1% silane start submerging in the water, as illustrated in Figure3 (b), implying their wettability changes with time. The physical reason for this observation is the formation of a critical thickness thin-film of methyl polysiloxanes that immediately coats the glass bead during the silanization process. We observe that the glass beads treated with 2% silane concentration sustain wettabil-

ity for a long time [80]. Therefore, we use 2% silane and 98% dehydrated toluene solution in the silanization reaction to alter the glass beads' wettability and call the treated glass beads oil-wet glass beads. Further, we perform a capillary rise experiment to quantify the wettability.

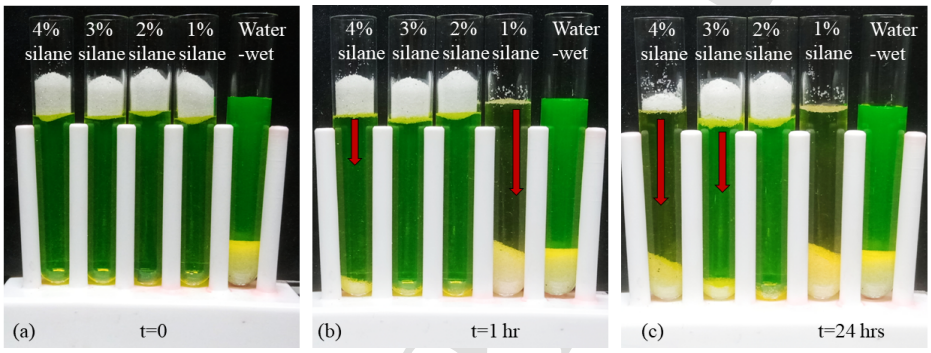

Figure 3: Images of the flotation test at times (a) t = 0, (b) t = 1 hour, and (c) t = 24 hours.

2.3. Capillary rise experiment

We perform the capillary rise experiment in a glass straw of 5 *mm* internal diameter and 30 *cm* length. We use Whatman filter paper at the bottom end of the tube for holding the glass beads. We fill the tubes with the water-wet glass beads, oil-wet glass beads, and mixture of 50% water-wet and 50% oil-wet glass beads i.e., mixed-wet glass beads. Figure 4 shows the capillary rise experimental setup and the maximum water rise through the glass beads packing after 24 *hours*. We observed 22 *cm* water rise in the water-wet glass beads, 15 *cm* in the mixed-wet glass bead and only 2.5 *cm* in the oil-wet glass beads. This experiment confirms the difference in the water-wet, mixed-wet

and oil-wet glass beads wettability.

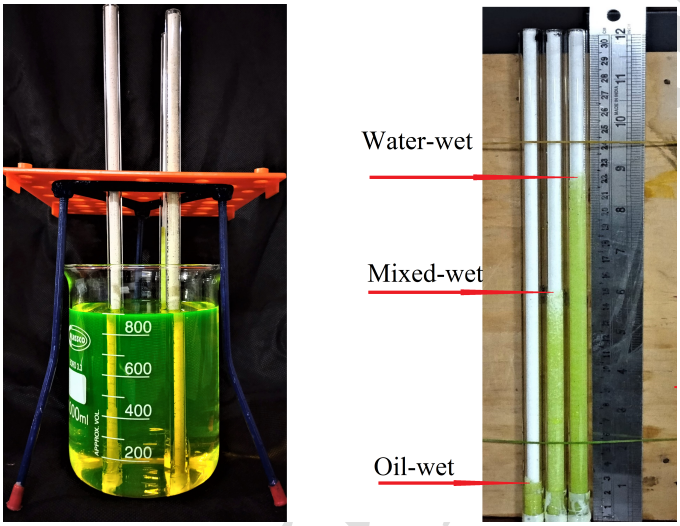

Figure 4: Left: experimental set-up for a capillary rise experiment. Right: the maximum water rise through the various wetting state glass beads packing after 24 hours.

Using the above-prepared glass beads, we now want to quantify the contact area of the glass beads with water during multiphase flow. For this, we now move to flow experiments.

3. Flow experiments with single-phase

Figure 2 shows our experimental setup. For the porous medium, we took an acrylic cylindrical tube with an inner diameter of 2 *cm* and a length of 15 *cm*. We packed the glass beads while intermittently tapping the tube for dense and uniform packing. We prevent the migration of glass beads out of the packing using Whatman filter paper on both ends of the tube. We use

a Cole-Parmer syringe pump for the liquid injection into the packed tube at a constant flow rate and set the continuous-time intervals in a GILSON-FC203B fraction collector to collect the exit stream. For the aqueous phase, we use FSS as a non-adsorbing or ideal tracer, and STS as an adsorbing tracer. The ideal tracer (FSS) follows the flow path and its mean residence time can give us the estimate of the pore volume or void volume in the porous medium. The adsorbing tracer (STS) dynamically adsorbs and desorbs on the porous solid surface which leads to a delay in the arrival of the tracer at the exit. Therefore, we see that the mean residence time of the adsorbing tracer is more than the non-adsorbing tracer as shown in Figure 1. The mean residence time of the tracer is identically equal to the first moment of the tracer concentration vs time curve for a pulse input of the tracer or the left-hand side of Eqn. (1) and Eqn. (2) for a step input of the tracer [75, 83].

$$\int_0^\infty \left(1 - \frac{C_{exit}(t)}{C_T}\right)_{ideal} dt \ = \tau_i = \frac{\phi\, V}{Q} \tag{1}$$

$$\int_0^\infty \left(1 - \frac{C_{exit}(t)}{C_T}\right)_{adsorbing} dt = \tau_a = \frac{\phi\, V}{Q} + \frac{K_a A_T}{Q} \tag{2}$$

where $C_{exit}(t)$ is the effluent tracer concentration with the time (g/l) [69, 57], and C_T is the injected tracer concentration (g/l). τ_i and τ_a are the mean residence times (min) of the ideal and adsorbing tracers, respectively. The mean residence time of the tracer can be estimated using the porous medium characteristics as well, which are given in the right-hand side of

the Eqn. (1) and Eqn. (2). Here, ϕ is the porosity of the medium, V is the bulk volume of the porous medium (ml), Q is the liquid flow rate (ml/min), K_a is the adsorption partition coefficient onto the solid matrix (ml/g), and A_T is the total mass of the glass beads in contact with the liquid (g) or liquid-solid interfacial area (m^2). For Eqn. (2), we assume [69]: (i) isothermal process (ii) negligible pressure variation (of the order 10^{-3} bar in our experiments) in the porous column. (iii) linear adsorption isotherm for the adsorbing tracer on the solid surface. (iv) instantaneous adsorption in comparison to flow time scale. The adsorbing water-tracer (STS) follows the linear adsorption isotherm and physically adsorbs [84] on the glass beads surface. We will show linear adsorption isotherm in our flow experiments. We analyse the FSS and STS concentrations in the effluent sample using a UV-visible spectrophotometer (UV-2700 SHIMADZU) at wavelength 490 nm and 215 nm, respectively [75]. To investigate the interaction of FSS and STS with the organic phase, if any, we analyse the UV-visible spectrum of FSS and STS dissolved in the aqueous-phase after mixing with the organic phase. In Figure 5 we show that FSS and STS do not interact with the organic-phase as their UV-Visible spectrum in the aqueous phase remains unchanged after vigorous mixing with the organic phase. Therefore, we use K_a as a constant for the aqueous-phase during the multiphase flow experiments.

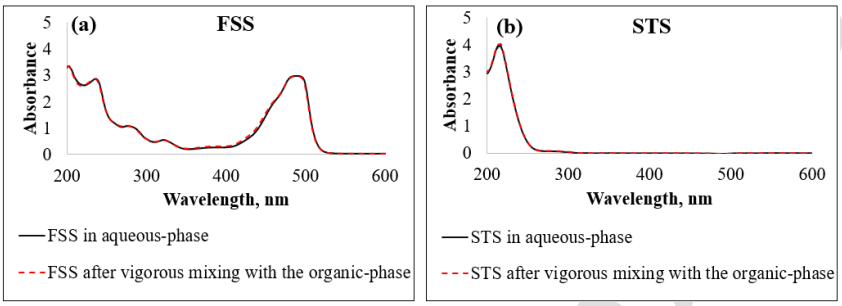

Figure 5: UV—visible spectrum of the tracer, in the aqueous-phase and after the mixing with the organic-phase.

In this study, we assume a constant surface area of the glass beads per unit weight and use A_T in the mass units (g). Using the Eqn. (1) and (2), with a known K_a, we can determine the fractional weight of the solid in contact with water (A_w/A_T) during multiphase flow. In a single-phase flow experiment, A_T is the entire surface of the porous matrix, which is wetted by the water. We use the single-phase flow experiments to estimate K_a in our system. In the single phase flow experiments with a known A_T, if the K_a is constant at different flow rates we can prove our assumption of linear adsorption isotherm and instantaneous adsorption in comparison to flow time scale.

3.1. Estimation of K_a using single-phase flow experiment

For single-phase flow experiments;

i First, we weigh the empty tube (A, g). Further, we weigh the tube packed with glass beads (B, g). The total weight of the glass beads packed in the tube is ($A_T = B - A, g$).

ii Initially, we arranged the glass beads' packed tube vertically, injected the Deionized water (DIW) from the bottom of the tube, and saturated the glass beads thoroughly with at least nine pore volumes of water.

iii After that, we perform a water-tracer flow experiment in the horizontal tube. We inject the ideal tracer (FSS) as a step-input at a particular flow rate until it is observed at the injected tracer concentration at the exit. We measure the effluent tracer concentration with time using a UV-vis spectrophotometer.

iv We now flush the ideal tracer using deionized water for at least five pore volumes so that there is no UV-vis spectrum visible in the effluent for FSS.

v Then, we inject the adsorbing tracer (STS) at the same flow rate as used for injection of the ideal tracer and measure the exit tracer concentration with time till the exit tracer concentration of the adsorbing tracer is the same as the inlet stream. After injecting the adsorbing tracer, we flush the tracer by injecting the DI water till no tracer is seen in the effluents under the UV-vis spectrophotometer. We perform tracer injection experiment; i.e., steps (iii) to (v), three times at one particular flow rate in the same packing of the glass beads for accuracy and repeatability of the tracer effluent history.

vi After completing the experiment at one particular flow rate and wettability, we weigh the tube (D, g) to estimate the amount of the trapped liquid in the pores $(E = D - B, g)$.

vii We calculate the porosity by $\phi = (\frac{E}{\rho_w})/V$ and pore volume ($PV = \phi V$) of the porous medium, where V is the bulk volume of the tube.

viii We repeat steps (iii) to (vii) at flow rates 0.25, 0.5, *and* 1 ml/min in the same porous medium.

Using Eqn. (1) and (2), with the known weight of the glass beads (A_T) and the pore volume (PV), we calculate the K_a of the adsorbing tracer in the system.

3.2. Estimation of K_a for STS

We do the water flow experiment with tracer-tests at flow rates 0.25, 0.5, and 1 ml/min at room temperature (25^0C) and atmospheric pressure for three wetting conditions i.e., water-wet (WW), oil-wet (OW), and mixed-wet (MW). We show in Figure 6, the FSS and the STS breakthrough curves at three flow rates and three wetting conditions. Figure 6 shows retardation of the STS compared to the FSS at every flow rate and wetting condition, due to the physical adsorption [84] of STS on the glass bead surface.

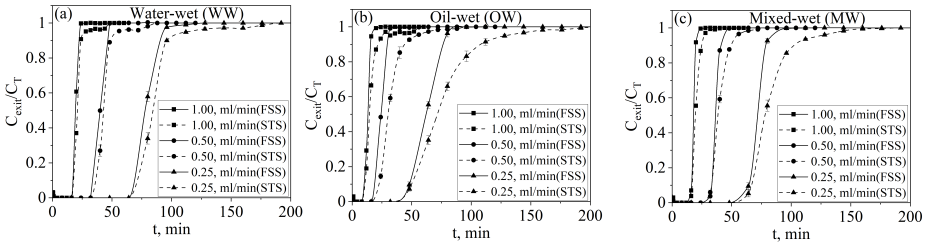

Figure 6: The tracer breakthrough curves from the single-phase flow experiment at various flow rates and wetting conditions (a) water-wet, (b) oil-wet, and (c) mixed-wet.

Using the tracer breakthrough curves in Figure 6, we first compare the experimental mean residence time (MRT) for the ideal tracer using the left side of Eqn. 1 with the theoretical MRT obtained from the process parameters ϕ, V, and Q on the right-side of Eqn. 1. Figure 7 shows an excellent match in the experimental and theoretical MRT for the ideal tracer at different flow rates and wetting conditions. Corresponding to the same flow rates and wetting conditions, we also show the experimental mean residence time of the adsorbing tracer (STS) calculated using the left-hand side of Eqn. 2. The adsorbing tracer shows a higher mean residence time due to adsorption on the glass beads surface.

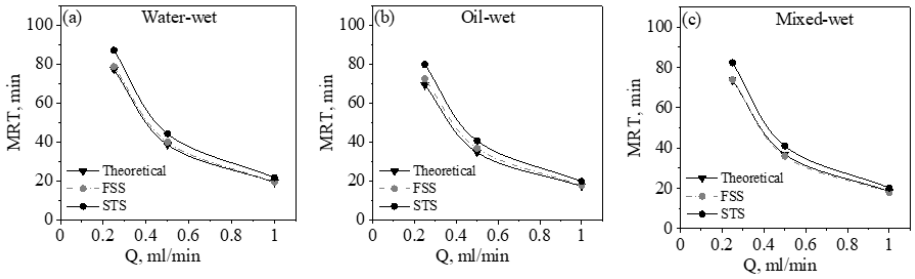

Figure 7: Comparison of theoretical MRT with the experimental MRT by the tracer breakthrough curves from the single-phase flow experiment at various flow rates and wetting conditions (a) water-wet,(b) oil-wet, and (c) mixed-wet.

We calculate the K_a of the STS at every flow rate and wetting conditions, using Eqn. (1) and Eqn. (2). In Table 2, we show the experimental mean residence times of the two tracers with process parameters and calculated K_a. We use the mean τ_i and τ_a obtained from the three repetitions of the tracer test for a given flow rate and wetting conditions in Eqn.(1) and (2)

to estimate K_a as given in the last column of Table 2. The K_a should be independent of the flow rates for the validity of Eqn.(2). The estimated K_a for water-wet, oil-wet, and mixed-wet are 0.027±0.001, 0.027±0.001, and 0.028± 0.001, respectively. However, K_a can depend on the surface chemical compositions. We analyze the compositions of such silane treated glass beads' surfaces by the X-Ray Diffraction (XRD). In Figure 8, we show the XRD of the oil-wet and water-wet glass beads and observe no such significant change in the surface composition of the glass beads after the silanization process. In further calculations, we use Ka = 0.027, which is the combined average.

Table 2: Estimated K_a from the single-phase flow experiments (V = 47.10 ml).

Wettability	Q, $\frac{ml}{min}$	ϕ	PV= ϕV	A_T, g	τ_i= $\int_0^\infty[1-\frac{C_{exit}(t)}{C_T}]dt$, min (FSS)	τ_a= $\int_0^\infty[1-\frac{C_{exit}(t)}{C_T}]dt$, min (STS)	$(\tau_a-\tau_i)\frac{Q}{A_T}$ =K_a, $\frac{ml}{g}$
WW	1.00	0.41	19.31	80.80	19.41±0.22	21.76±0.31	**0.029**
	0.50	0.41	19.31	80.80	40.00±0.31	44.27±0.27	**0.026**
	0.25	0.41	19.31	80.80	78.78±0.24	87.15±0.28	**0.026**
OW	1.00	0.37	17.33	73.46	17.67±0.28	19.77±0.31	**0.029**
	0.50	0.37	17.38	73.46	36.81±0.24	40.63±0.29	**0.026**
	0.25	0.37	17.38	73.46	72.50±0.24	79.87±0.20	**0.025**
MW	1.00	0.39	18.42	74.02	18.00±0.23	20.20±0.41	**0.030**
	0.50	0.39	18.42	74.02	36.97±0.55	41.02±0.45	**0.027**
	0.25	0.39	18.42	74.02	74.00±0.53	82.37±0.49	**0.028**

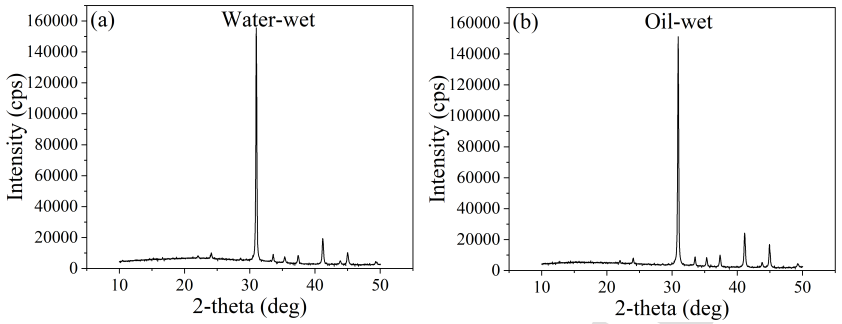

Figure 8: X-Ray Diffraction (XRD) of the (a) water-wet, and (b) oil-wet glass beads at 10-50 degree diffraction.

Now, we use the estimated K_a in the two-phase flow experiments for quantifying the water wetted surface area of the glass beads at different flow rates and wetting conditions.

4. Flow experiments with two-phases

We use the single-phase flow experiments set up to perform the two-phase flow experiments. To reiterate, we consider a constant interfacial area for unit mass for all the beads, therefore, mass units are used for area. Single-phase flow experiments ended with the injection of adsorbing water tracer. To remove the adsorbing water-tracer, we inject five pore-volume of DI water. We then displace the water in the glass beads packing with oil at a 1 ml/min flow rate. This gives us a porous packing with initial oil saturation and some remaining water saturation. This condition is similar to the initial subsurface oil reservoir condition where we have connate water and oil. Once we

reach steady-state and only oil is present in the exit stream, we use the mass balance to find the connate water saturation (S_{wc}) or the initial water saturation in the packing, which is noted in Table 3 column 4. Then we again inject water to displace oil, i.e., secondary imbibition at a low flow rate of 0.25 ml/min for all wetting conditions. We collect the exit stream in the tubes arranged in a fraction collector at a constant interval till steady-state. In Figures 9 (a) and (b), we show the collected exit streams in the tubes (left to right) at a constant interval and the total volume of the oil displaced from the water during secondary imbibition for different wetting conditions, respectively. We use the mass balance to calculate the residual volume of the oil after the secondary imbibition.

Further, we calculate the oil recovery factor using the ratio of the displaced volume of oil during secondary imbibition and the initial volume of the oil in the porous medium. In Figure 9 (c), we show the ultimate oil recovery vs time curve measured at 0.25 ml/min from the different wetting conditions. We recovered 82%, 58%, and 31% of the oil from the water-wet, mixed-wet, and oil-wet porous medium, respectively. These result also show the wettability alteration of the glass beads. When we reach a steady state for the secondary imbibition and the exit stream has only water, the oil is at the residual saturation at this point. We now perform the tracer experiments by following the steps (iii) to (v) as described above in Section 3.1.

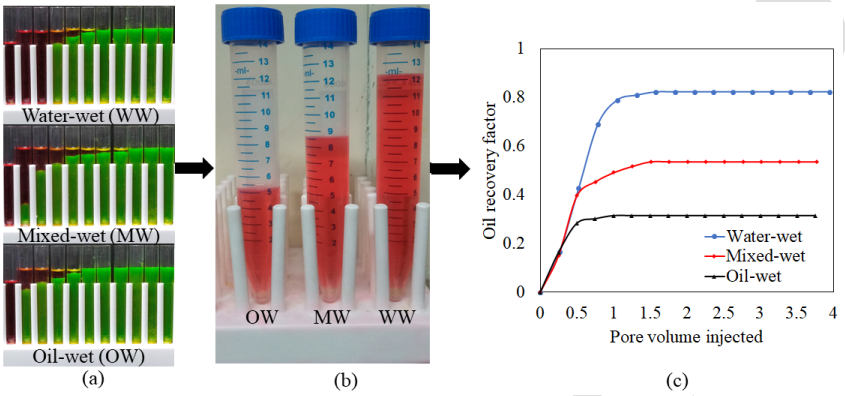

Figure 9: (a) Collected samples of the steady exit streams at a constant time interval left to right tube (Red liquid is oil and green liquid is water) (b) The total volume of the oil displaced from the water during secondary imbibition from different wetting conditions (c) Profile of the ultimate oil recovery rate by secondary water imbibition mechanism at 0.25 ml/min from the various wetting conditions of the glass beads packing.

We calculate the MRTs of the FSS and STS at the residual oil saturation, using left hand side of Eqn. (3) and (4).

$$\int_0^\infty \left(1 - \frac{C_{exit}(t)}{C_T}\right)_{ideal} dt \; = \tau_{ii} = \frac{\phi V S_i}{Q} \tag{3}$$

$$\int_0^\infty \left(1 - \frac{C_{exit}(t)}{C_T}\right)_{adsorbing} dt \; = \tau_{aa} = \frac{\phi V S_i}{Q} + \frac{K_a A_w}{Q} \tag{4}$$

where $C_{exit}(t)$ is the effluent tracer concentration (g/l) with the time, and C_T is the injected tracer concentration (g/l), measured using UV-vis spectrophotometer at various times. τ_{ii} and τ_{aa} represents the mean residence time of the ideal tracer and the adsorbing tracer (min), respectively, when residual oil is present in the porous medium. S_i is the mobile-phase or water saturation and A_w is the solid-water interfacial area (g).

Using Eqns. (3) and (4), with the estimated K_a from the single-phase experiment, we can calculate the water-solid interfacial area (A_w) during the two-phase flow in the porous medium.

Once three repetitions of the tracer experiments are completed at the water flow rate of 0.25 ml/min, we increase the water injection rate to 0.5 ml/min. Extra oil is recovered from the packing when the flow rate is increased, which is used to find the new residual saturation of oil at a 0.5 ml/water injection rate. We perform three sets of tracer experiments at a 0.5 ml/min water injection rate and then increase the water injection rate to 1 ml/min. We then repeat all the steps at 1 ml/min injection rate. Therefore, for a given wettability of the glass beads, we use the same packing for all the experiments for consistency. We change the packing for oil-wet and mixed-wet glass beads.

4.1. Estimation of solid-water interfacial area A_w

In Figure 10, we show the tracer breakthrough curves at various flow rates of water and different wetting conditions. Oil is the residual-phase in the experiments and does not flow. Comparing Figure 10 and Figure 6, we see the early arrival of the ideal tracer during the two-phase flow experiments due to the presence of the residual oil in the porous medium. We measure the water saturation (S_w) in the two-phase system by the ratio of the ideal

tracer MRT during the two-phase to the single-phase flow in the porous medium from Eqn. (3) and (1). The S_w calculated using the mass balance and the MRTs show an excellent match for the water-wet and mixed-wet conditions as listed in the column 5 and 8 of Table 3. However, we observe a slight variation for the oil-wet condition. This may be due to some immobile pockets of water formed at low flow rates, which are not captured in the tracer experiments. Therefore, we use mass balance saturation in our calculations.

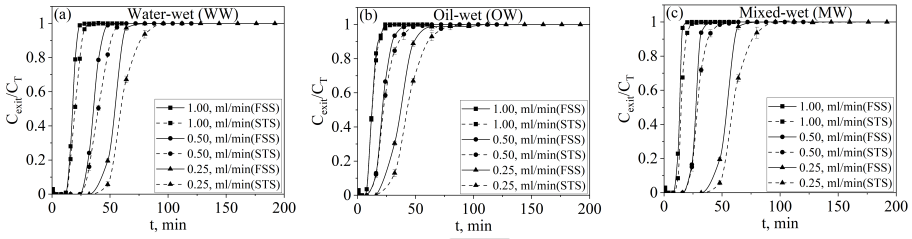

Figure 10: Tracer breakthrough curve during two-phase flow experiments, when oil is the residual-phase in the experiments and does not flow at various flow rates and wetting conditions (a) water-wet, (b) oil-wet, and (c) mixed-wet.

In Figure 11, we show the irreducible oil saturation (S_{ro}) measured using mass balance after secondary imbibition at various flow rates for the different wetting conditions. These results align with our expectations of having high oil recovery at a high flow rate and more water wetting conditions. We also observe that wettability has more prominent influence on the ultimate oil recovery as seen from the residual oil saturation in comparison to the flow rate. We now estimate the A_w using the MRTs of the adsorbing and the non-adsorbing tracers at three different flow rates (1, 0.5, and 0.25 ml/min) and

three wetting conditions (water-wet, oil-wet, and mixed-wet) as presented in Table 3, when oil is the residual-phase.

Table 3: The estimated interfacial area of the glass beads in contact with water (A_w), when oil (DD) is the residual-phase at different flow rates and different wetting conditions (V = 47.10 ml, K_a= 0.027,ml/g).

Wettability	Flow rate (Q), $\frac{ml}{min}$	A_T, g	S_{wc}, (MB)	S_w (MB)	τ_{ii} (FSS), min	τ_{aa} (STS), min	$S_w = \frac{\tau_{ii}}{\tau_i}$	S_o = 1-S_w	$A_w = (\tau_{aa} - \tau_{ii})\frac{Q}{K_a}$, g	$\frac{A_w}{A_T}$
WW	1.00	80.80	–	0.86	16.93±0.32	19.28±0.22	0.87	0.13	78.17	0.97
	0.50	80.80	–	0.85	34.50 ±0.25	39.00±0.23	0.86	0.14	75.00	0.93
	0.25	80.80	0.26	0.83	65.38±0.22	73.33 ±0.21	0.83	0.17	65.58	0.82
OW	1.00	73.46	–	0.64	11.15±0.32	12.59±0.32	0.63	0.37	48.00	0.65
	0.50	73.46	–	0.60	19.84 ±0.35	23.01±0.32	0.54	0.46	52.75	0.72
	0.25	73.46	0.19	0.54	36.43±0.32	43.25±0.41	0.50	0.50	56.83	0.77
MW	1.00	74.02	–	0.76	13.54±0.22	15.46±0.24	0.75	0.25	64.00	0.86
	0.50	74.02	–	0.74	26.70 ±0.20	30.40±0.22	0.74	0.26	61.67	0.83
	0.25	74.02	0.24	0.73	54.75±0.26	61.86 ±0.21	0.74	0.26	60.42	0.80

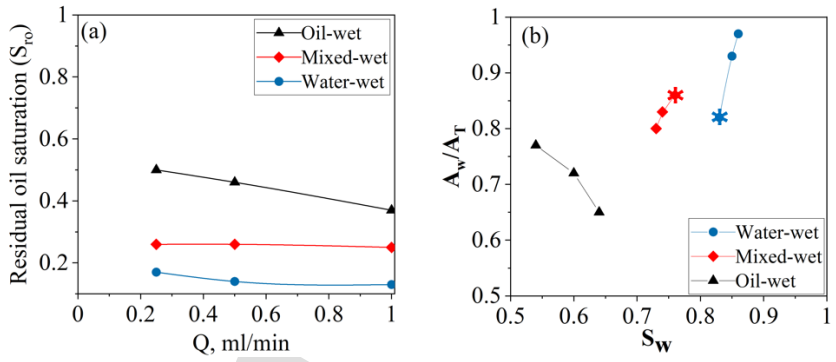

Figure 11: (a) Flow rate versus residual oil saturation in the different wetting condition porous medium and (b) Relationship between the fraction of the glass beads surface area in contact with water (A_w/A_T) and the water saturation (S_w), when oil is the residual-phase.

Figure 11 (b) shows the fraction of the total area that is wetted with water vs saturation of water curves for different wetting conditions. For the water-wet case, we see that at a slow flow rate of water, we get low saturation of water and low contact area. As we increase the flow rate, the water-solid

area increases steeply with the saturation. This is because, water may flow into pore boundaries increasing the contact area more than the saturation. Mixed-wet beads follow a similar trend; however, changes in contacted area and saturations are lower than in the water-wet case. Comparing the water-wet and the mixed-wet cases, the highest water saturation in the mixed-wet beads is lower than the lowest water saturation in the water-wet beads shown by the starred points in Figure 11 (b). In contrast, comparing the contact area of water with the solid at these starred points, the water-solid interfacial area is higher in the mixed-wet beads than in the water-wet beads. This is because the flow rate is different at the two points, which affects the capillary number and the wetting condition of the beads. Pore-scale studies are required to understand further if the corner flow is more pronounced in mixed-wet beads at higher capillary numbers. In the oil-wet case, we see an interesting trend that as the saturation of water increases, the solid-water interfacial area decreases. A similar result has been observed by Jain et al. [68] for the fluid-fluid interfacial area estimation in the oil-wet porous medium. Zhao et al. [76] show that for the oil-wet case, when we increase the capillary number by increasing the flow rate, the displacement may become unstable due to a finger-like front and the fraction of the oil displaced from a pore may also decrease. Now, we are increasing the flow rate sequentially. Therefore, when we increase the flow rate, readjustment of the fluids leads to more oil recovery; however, at high flow rate, more oil is present at the pore boundaries leading to the less solid-water interfacial area. Further,

Figure 12 illustrate a macro-scale view of the submerged water-wet glass beads (1 g), oil-wet glass beads (1 g), and mixed-wet glass beads (0.5 g WW + 0.5 g OW) in water. We note that the oil-wet glass beads form aggregates inside the water due to their hydrophobic nature unlike the water-wet beads leading to the anomalous behaviour seen in solid-water interfacial area vs water saturation curve for oil-wet surface.

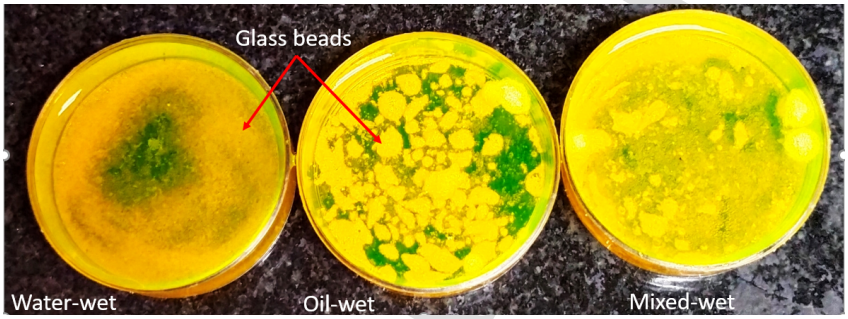

Figure 12: Water-wet, Oil-wet and Mixed-wet glass beads' behaviour in contact with water.

4.2. Flow experiment with two flowing phases

We now perform the two-phase flow experiments when oil and water flow simultaneously through the porous medium. We use the same setup from Section 4.1, where the experiments ended with water being injected at a flow rate of 1 ml/min. We now use two syringe pumps to inject the oil and water simultaneously into the same system, as shown in Figure 2. We maintain a total flow rate of 1 ml/min into the porous medium using different water and oil flow rates. To first remove the tracers, we inject five pore-volume of DI water. Then we decrease the water flow rate to 0.75 ml/min and start

injecting oil at a flow rate of 0.25 ml/min. Once the steady-state is reached, that is, at the exit we are producing water at a flow rate of 0.75 and oil at a rate of 0.25 ml/min, we start the water-tracer experiment following the steps (iii) to (v) as described in Section 3.1. We then decrease the water injection rate to 0.5 ml/min and then to 0.25 ml/min and increase the oil flow rate to 0.5 ml/min and then to 0.75 ml/min to keep the total flow rate 1 ml/min. We do the water-tracer experiment after reaching steady-state at every flow condition. We calculate A_w, using Eqn. (3) and (4) with the estimated K_a from the single-phase flow experiment.

In Figure 13, we show the tracer breakthrough curves for the above experiments when both oil and water are simultaneously flowing through the porous medium at various flow rates. We report the estimated A_w at different water flow rates and wetting conditions in Table 4. We obtain a monotonic increasing behaviour of the water-saturation with the water flow rates for all the wetting conditions, as shown in Figure 14 (a). We observe that the increase in the water saturation with flow rate is more for the water-wet than for the oil-wet case. This is because, in the oil-wet porous medium, water flows through the easiest paths, with the larger pore-bodies and leaving a large oil in the system [85]. Figure 14 (b) illustrates the behaviour of the quantified solid-water interfacial area with the water saturation during the continuous two-phase flow at the three wetting conditions of the porous medium. We find that the oil-wet porous medium gives less solid-water interfacial area

at the same saturation than the other wetting conditions: water-wet and mixed-wet, as is expected. Here, we observe that in the oil-wet case, the increase in the fractional water-solid interfacial area is more pronounced when the water saturation increases than for water-wet case. This is because, the water move through small pores or pore boundaries in the water-wet case and as the water saturation increases it starts invading larger pores which have less surface area per unit void volume. However, for the oil-wet case the phenomena reverses.

On the whole, we find differences in the behaviour of the water-solid interfacial area with water saturation when experiments are done at the residual oil saturation and when both the phases are flowing. At the residual oil saturation, an increase in water saturation leads to a proportionately more increase in the water-solid interfacial area for water-wet beads while the interfacial decreases for the oil-wet case. When both fluids are flowing, then for the oil-wet case, the water-solid interfacial area increases more than the water-wet case at higher water saturations. However, the water saturation increase is not as high as in the water-wet case. This is because of the viscous fingering instability in the water-wet and oil-wet medium at different flow rates [86].

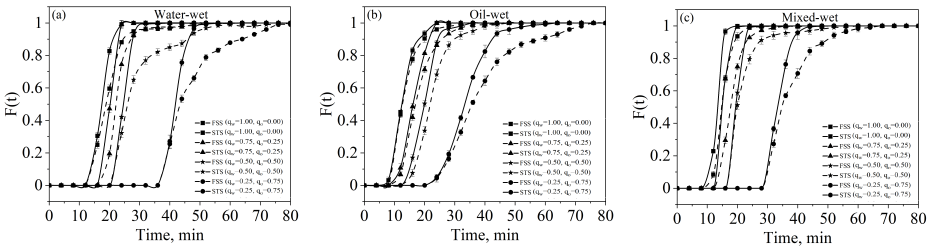

Figure 13: Tracer breakthrough curve when both oil and water are simultaneously flowing through the glass beads packing at various flow rates and wetting conditions (a) water-wet, (b) oil-wet, and (c) mixed-wet.

Table 4: Estimation of the fraction of solid-water interfacial area (A_w/A_T) when oil and water are simultaneously flowing through the porous medium at different wetting conditions (V = 47.10 ml, K_a= 0.027,ml/g).

Wetability	q_w, $\frac{ml}{min}$	q_o, $\frac{ml}{min}$	S_w= $\frac{\tau_{ii}}{\tau_i}$	τ_{ii} (FSS), min	τ_{aa} (STS), min	A_T, g	A_w= $(\tau_{aa}-\tau_{ii})\frac{f_w}{K_a}$, g	$\frac{A_w}{A_T}$
WW	1.00	0.00	0.87	16.89±0.10	19.24±0.09	80.80	78.38	0.97
	0.75	0.25	0.79	20.28±0.12	23.38±0.13	80.80	77.57	0.96
	0.50	0.50	0.59	23.60±0.14	27.58±0.12	80.80	66.26	0.82
	0.25	0.75	0.49	38.60±0.21	43.84±0.25	80.80	43.63	0.54
OW	1.00	0.00	0.71	12.56±0.19	13.86±0.22	73.46	43.34	0.59
	0.75	0.25	0.70	16.00±0.28	17.68±0.28	73.46	41.87	0.57
	0.50	0.50	0.67	24.66±0.28	26.73±0.25	73.46	34.53	0.47
	0.25	0.75	0.55	39.88±0.23	42.78±0.37	73.46	24.24	0.33
MW	1.00	0.00	0.75	13.54±0.18	15.46±0.12	74.02	64.00	0.86
	0.75	0.25	0.67	15.74±0.15	18.19±0.20	74.02	61.34	0.83
	0.50	0.50	0.56	20.15±0.22	22.65±0.20	74.02	41.62	0.56
	0.25	0.75	0.50	37.00±0.21	41.03±0.27	74.02	33.59	0.45

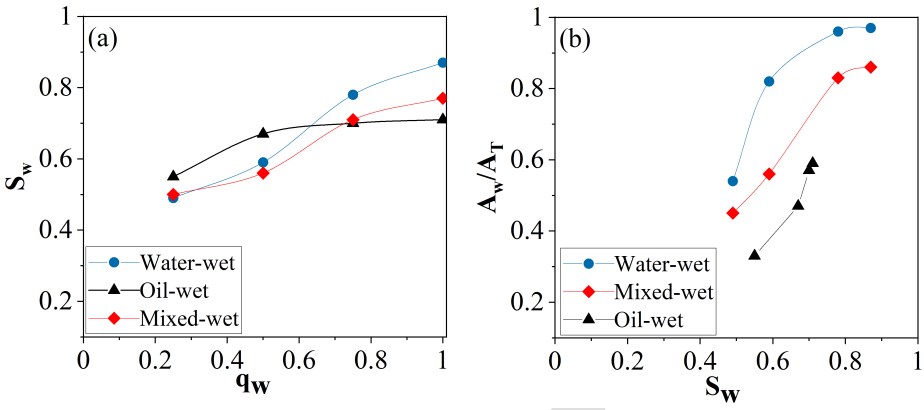

Figure 14: Relationship between the water flow rate with (a) water-saturation, when oil and water simultaneously flowing through the porous medium. (b) Behaviour of the quantified solid-liquid interfacial area at various saturation through different wetting conditions porous medium.

5. Validity of the methodology for geological system

Further, we investigate the presented method to directly quantify the wetted area of the solid by a liquid during the multiphase flow in a sand-pack. This is because the natural porous medium is similar to sand in many cases, and it is challenging to control for morphology or chemistry [87]. We use the quartz sand, with a bulk density of $1.77 \pm 0.01 g/cm^3$ and an average grain diameter of 200 μm in its original state as purchased from GLR innovators New Delhi, India. We follow the step by step procedure for estimating the solid-water interfacial area as discussed above in the glass beads packing. First, we perform the single-phase flow experiments with water-tracer at flow rates 0.25, 0.5, and 1 ml/min and compare the theoretical MRT of the tracer with the experimental MRT.

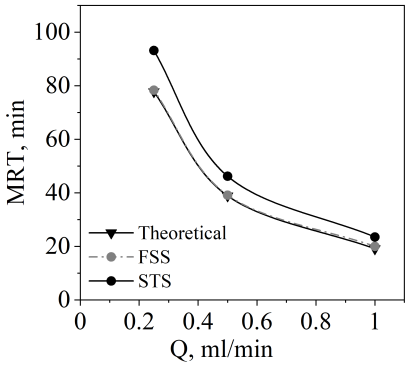

Figure 15: Comparison of theoretical MRT with the experimental MRT of the tracer break-through curves from the single-phase flow experiment at various flow rates in sand pack.

Figure 15 shows an excellent match in experimental and theoretical MRT for the ideal tracer. We also obtain a higher mean residence time of the adsorbing tracer (STS) corresponding to the same flow rates due to the adsorption on the sand surface. Further, we estimate K_a at every flow rate and the calculated data we present in Table 5. Sand typically have irregular grains and rough surface, which promote corner flow [17] and can affect the K_a values. Therefore, we use the calculated K_a at a particular flow rate for the A_w measurement during the two-phase flow experiments in the sand-pack.

Table 5: Estimated K_a from the single-phase flow experiments (V=47.10 ml).

Q, $\frac{ml}{min}$	ϕ	PV= ϕV	A_T, g	τ_i= $\int_0^\infty[1-\frac{C_{exit}(t)}{C_T}]dt$, min (FSS)	τ_a= $\int_0^\infty[1-\frac{C_{exit}(t)}{C_T}]dt$, min (STS)	$(\tau_a-\tau_i)\frac{Q}{A_T}$ $=K_a$, $\frac{ml}{g}$
1.00	0.41	19.31	79.43	19.94±0.12	23.50±0.26	**0.045**
0.50	0.41	19.31	79.43	39.13±0.21	46.21±0.28	**0.045**
0.25	0.41	19.31	79.43	78.36±0.24	93.18±0.28	**0.047**

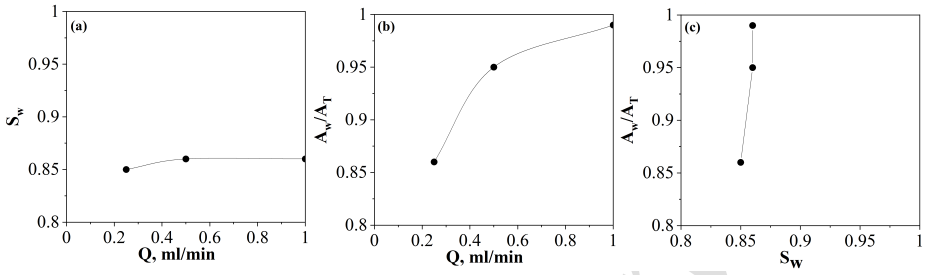

Figure 16: Two-phase flow experiment, when oil is the residual-phase in the experiments and does not flow at various flow rates and only water is the mobile-phase in the sand pack.

Further, we perform a two-phase flow experiment when water is mobile, and oil is residual. Figure 16 shows experimental results during two-phase flow in the sand-pack. From these figures, we observe water-saturation (Figure 16(a)) and solid-water interfacial area (Figure 16(b)) are directly proportional to the water flow rate because it includes the maximum pore area of the grain at a higher water flow rate. It is as expected because corner flow plays an important role in strong imbibition in natural porous media like sand [17]. We can compare Figure 16(c) with Figure 10(b) for the measured A_w/A_T at different water saturations S_w. We obtain a similar monotonic increasing relationship between the water-saturation and solid-liquid interfacial area, though more A_w/A_T in the sand pack than in the glass bead pack. This is because of the surface roughness of the sand [87].

6. Conclusions

We explored the two-tracer technique and performed a series of experiments with ideal and adsorbing tracer to estimate the water-solid interfacial areas at different saturations, wetting conditions (water-wet, mixed-wet, and oil-wet), and the flow conditions. We found that when only water is flowing then for the (i) water-wet case the water-solid interfacial area increases with water saturation (ii) mixed wet case the water-solid interfacial increases with water saturation, however, the increase is not as pronounced as in the water-wet case (iii) oil-wet case the water-solid interfacial area decreases with increase in saturation of water. This may be due to rearrangement of the water and oil phases at different injection rates of water which we use to change the residual oil phase saturation in the oil-wet porous medium. In the range of saturations we explored, we find that the solid-water interfacial area depends on the capillary number and the contact angle and fluid saturations. When we did experiments for oil and water as flowing phases, then we observed that the water-wet case has more water-solid interfacial area at a given saturation than the mixed-wet case. The oil-wet case shows the least water-solid interfacial area at a given saturation. However, the rate of change of the interfacial area with the saturation varies in these cases which can be explained by pore scale phenomena at different flow rates and the wettability of the glass beads. These results can be further used to investigate a function of wettability dependent flow and saturation conditions for the geological systems.

Acknowledgement The authors thank the Board of Research in Nuclear Sciences, Department of Atomic Energy, India for financial support, project number: 35/14/50/2014-BRNS.

Nomenclature

A_T	Total glass beads surface area or total amount of the glass bead (g)
C_{exit}	Effluent tracer concentration (mol/dm^3)
C_T	Input tracer concentration (mol/dm^3)
K_a	Adsorption partition coefficient (ml/g)
ϕ	Porosity of the bed pack
Q	Volumetric liquid flow rate (ml/min)
q_w	Volumetric water flow rate (ml/min)
ρ_w	Density of the water (g/dm^3)
τ_i	Mean residence time of the ideal tracer (min)
τ_a	Mean residence time of the adsorbing tracer (min)
A_w	Total amount of the glass bead in contact with water(g)
A_o	Total amount of the glass bead in contact with oil (g)
V	Bulk volume of the porous substrate (ml)
S_o	Oil saturation
S_{ro}	Residual oil saturation
S_w	Water saturation
S_{cw}	Connate water saturation

References

[1] A. Mirzaei-Paiaman, M. Faramarzi-Palangar, S. Djezzar, S. Kord, A new approach to measure wettability by relative permeability measurements, Journal of Petroleum Science and Engineering 208 (2022) 109191.

[2] R. Ehrlich, H. Hasiba, P. Raimondi, Alkaline waterflooding for wettability alteration-evaluating a potential field application, Journal of Petroleum Technology 26 (12) (1974) 1335–1343.

[3] R. I. Al-Raoush, Impact of wettability on pore-scale characteristics of residual nonaqueous phase liquids, Environmental science & technology 43 (13) (2009) 4796–4801.

[4] C. Dai, Y. Chang, Y. Sun, Z. Yu, X. Sun, F. Ding, X. Ding, Mechanism of the wettability impact on surfactant imbibition in dodecane-saturated tight sandstone, Energy & Fuels 34 (6) (2020) 6862–6870.

[5] B. Ju, T. Fan, Z. Li, Improving water injectivity and enhancing oil recovery by wettability control using nanopowders, Journal of Petroleum Science and Engineering 86 (2012) 206–216.

[6] S. I. Hwang, K. P. Lee, D. S. Lee, S. E. Powers, Effects of fractional wettability on capillary pressure–saturation–relative permeability relations of two-fluid systems, Advances in water resources 29 (2) (2006) 212–226.

[7] T. Akyazi, L. Basabe-Desmonts, F. Benito-Lopez, Review on microflu-

idic paper-based analytical devices towards commercialisation, Analytica chimica acta 1001 (2018) 1–17.

[8] N. R. Morrow, Wettability and its effect on oil recovery, Journal of petroleum technology 42 (12) (1990) 1476–1484.

[9] B. D. v. Woudt, Particle coatings affecting the wettability of soils, Journal of Geophysical Research 64 (2) (1959) 263–267.

[10] D. Tian, Y. Song, L. Jiang, Patterning of controllable surface wettability for printing techniques, Chemical society reviews 42 (12) (2013) 5184–5209.

[11] A. Singhal, P. Dranchuk, Wettability control of glass beads, The Canadian Journal of Chemical Engineering 53 (1) (1975) 3–8.

[12] V. Joekar-Niasar, S. Hassanizadeh, Analysis of fundamentals of two-phase flow in porous media using dynamic pore-network models: A review, Critical reviews in environmental science and technology 42 (18) (2012) 1895–1976.

[13] M. Yao, L. D. Tijing, G. Naidu, S.-H. Kim, H. Matsuyama, A. G. Fane, H. K. Shon, A review of membrane wettability for the treatment of saline water deploying membrane distillation, Desalination 479 (2020) 114312.

[14] M. Rücker, W.-B. Bartels, G. Garfi, M. Shams, T. Bultreys, M. Boone, S. Pieterse, G. Maitland, S. Krevor, V. Cnudde, et al., Relationship

between wetting and capillary pressure in a crude oil/brine/rock system: From nano-scale to core-scale, Journal of colloid and interface science 562 (2020) 159–169.

[15] S. Marsden, Wettability: its measurement and application to water-flooding, Sekiyu Gijutsu Kyokaishi;(Japan) 30 (1) (1965).

[16] E. Ionescu, B. Maini, A review of laboratory techniques for measuring wettability of petroleum reservoir rocks (1983).

[17] F. A. Dullien, Porous media: fluid transport and pore structure, Academic press, 2012.

[18] H. R. Warner, The reservoir engineering aspects of waterflooding, Society of Petroleum Engineers, 2015.

[19] W. G. Anderson, Wettability literature survey-part 1: rock/oil/brine interactions and the effects of core handling on wettability, Journal of petroleum technology 38 (10) (1986) 1125–1144.

[20] W. Anderson, Wettability literature survey-part 2: Wettability measurement, Journal of petroleum technology 38 (11) (1986) 1246–1262.

[21] W. G. Anderson, Wettability literature survey-part 3: the effects of wettability on the electrical properties of porous media, Journal of Petroleum Technology 38 (12) (1986) 1371–1378.

[22] W. G. Anderson, Wettability literature survey-part 4: Effects of wettability on capillary pressure, Journal of petroleum technology 39 (10) (1987) 1283–1300.

[23] W. G. Anderson, Wettability literature survey part 5: the effects of wettability on relative permeability, Journal of Petroleum Technology 39 (11) (1987) 1453–1468.

[24] W. G. Anderson, Wettability literature survey-part 6: the effects of wettability on waterflooding, Journal of petroleum technology 39 (12) (1987) 1605–1622.

[25] B. Ji, X. Sui, Q. Wang, Q. Li, L. Anjian, T. Liu, Advance on the tracer test technology among wells, in: SPE Asia Pacific Oil and Gas Conference and Exhibition, Society of Petroleum Engineers, 2002.

[26] A. Golparvar, Y. Zhou, K. Wu, J. Ma, Z. Yu, A comprehensive review of pore scale modeling methodologies for multiphase flow in porous media, Advances in Geo-Energy Research 2 (4) (2018) 418–440.

[27] Q. Lin, B. Bijeljic, S. Berg, R. Pini, M. J. Blunt, S. Krevor, Minimal surfaces in porous media: Pore-scale imaging of multiphase flow in an altered-wettability bentheimer sandstone, Physical Review E 99 (6) (2019) 063105.

[28] M. L. Brusseau, M. Narter, H. Janousek, Interfacial partitioning tracer test measurements of organic-liquid/water interfacial areas: application

to soils and the influence of surface roughness, Environmental science & technology 44 (19) (2010) 7596–7600.

[29] J. B. Araújo, M. L. Brusseau, Novel fluid–fluid interface domains in geologic media, Environmental Science: Processes & Impacts 21 (1) (2019) 145–154.

[30] R. T. Armstrong, J. E. McClure, M. A. Berrill, M. Rücker, S. Schlüter, S. Berg, Beyond darcy's law: The role of phase topology and ganglion dynamics for two-fluid flow, Physical Review E 94 (4) (2016) 043113.

[31] Z. Liu, A. Herring, C. Arns, S. Berg, R. T. Armstrong, Pore-scale characterization of two-phase flow using integral geometry, Transport in Porous Media 118 (1) (2017) 99–117.

[32] J. E. McClure, M. A. Berrill, W. G. Gray, C. T. Miller, Influence of phase connectivity on the relationship among capillary pressure, fluid saturation, and interfacial area in two-fluid-phase porous medium systems, Physical Review E 94 (3) (2016) 033102.

[33] J. E. McClure, R. T. Armstrong, M. A. Berrill, S. Schlüter, S. Berg, W. G. Gray, C. T. Miller, Geometric state function for two-fluid flow in porous media, Physical Review Fluids 3 (8) (2018) 084306.

[34] G. Garfi, C. M. John, Q. Lin, S. Berg, S. Krevor, Fluid surface coverage showing the controls of rock mineralogy on the wetting state, Geophysical Research Letters 47 (8) (2020) e2019GL086380.

[35] V. Joekar-Niasar, S. Hassanizadeh, A. Leijnse, Insights into the relationships among capillary pressure, saturation, interfacial area and relative permeability using pore-network modeling, Transport in porous media 74 (2) (2008) 201–219.

[36] A. L. Herring, E. J. Harper, L. Andersson, A. Sheppard, B. K. Bay, D. Wildenschild, Effect of fluid topology on residual nonwetting phase trapping: Implications for geologic co2 sequestration, Advances in Water Resources 62 (2013) 47–58.

[37] M. Andrew, B. Bijeljic, M. J. Blunt, Pore-scale imaging of geological carbon dioxide storage under in situ conditions, Geophysical Research Letters 40 (15) (2013) 3915–3918.

[38] S. Berg, H. Ott, S. A. Klapp, A. Schwing, R. Neiteler, N. Brussee, A. Makurat, L. Leu, F. Enzmann, J.-O. Schwarz, et al., Real-time 3d imaging of haines jumps in porous media flow, Proceedings of the National Academy of Sciences 110 (10) (2013) 3755–3759.

[39] M. Andrew, B. Bijeljic, M. J. Blunt, Pore-scale contact angle measurements at reservoir conditions using x-ray microtomography, Advances in Water resources 68 (2014) 24–31.

[40] G. Garfi, C. M. John, S. Berg, S. Krevor, The sensitivity of estimates of multiphase fluid and solid properties of porous rocks to image processing, Transport in Porous Media 131 (3) (2020) 985–1005.

[41] M. Prodanovic, W. B. Lindquist, R. S. Seright, Residual fluid blobs and contact angle measurements from x-ray images of fluid displacement, in: XVI International Conference on Computational Methods in Water Resources, Copenhagen, Denmark, 2006.

[42] G. Schnaar, M. Brusseau, Pore-scale characterization of organic immiscible-liquid morphology in natural porous media using synchrotron x-ray microtomography, Environmental science & technology 39 (21) (2005) 8403–8410.

[43] M. L. Brusseau, S. Peng, G. Schnaar, A. Murao, Measuring air- water interfacial areas with x-ray microtomography and interfacial partitioning tracer tests, Environmental science & technology 41 (6) (2007) 1956–1961.

[44] A. Russo, M. Narter, M. Brusseau, Characterizing pore-scale dissolution of organic immiscible liquid in a poorly-sorted natural porous medium, Environmental science & technology 43 (15) (2009) 5671–5678.

[45] M. L. Brusseau, M. Narter, G. Schnaar, J. Marble, Measurement and estimation of organic-liquid/water interfacial areas for several natural porous media, Environmental science & technology 43 (10) (2009) 3619–3625.

[46] M. Christensen, Y. Tanino, Waterflood oil recovery from mixed-wet

limestone: dependence upon the contact angle, Energy & Fuels 31 (2) (2017) 1529–1535.

[47] M. A. Tabar, M. H. Ghazanfari, A. D. Monfared, Compare numerical modeling and improved understanding of dynamic sessile drop contact angle analysis in liquid-solid-gas system, Journal of Petroleum Science and Engineering 184 (2020) 106552.

[48] A. Valori, B. Nicot, A review of 60 years of NMR wettability, Petrophysics 60 (02) (2019) 255–263.

[49] S. Tandon, C. Newgord, Z. Heidari, Wettability quantification in mixed-wet rocks using a new NMR-based method, SPE Reservoir Evaluation & Engineering (2020).

[50] Y. Zhang, Z. Li, F. Lai, H. Wu, G. Mao, C. D. Adenutsi, Experimental investigation into the effects of fracturing fluid-shale interaction on pore structure and wettability, Geofluids 2021 (2021).

[51] N. Ramskill, A. Sederman, M. Mantle, M. Appel, H. de Jong, L. Gladden, In situ chemically-selective monitoring of multiphase displacement processes in a carbonate rock using 3d magnetic resonance imaging, Transport in Porous Media 121 (1) (2018) 15–35.

[52] E. Toumelin, C. Torres-Verdín, B. Sun, K.-J. Dunn, Limits of 2d NMR interpretation techniques to quantify pore size, wettability, and fluid type: a numerical sensitivity study, Spe Journal 11 (03) (2006) 354–363.

[53] Y. Du, L. Guan, Interwell tracer tests: lessons learnted from past field studies, in: SPE Asia Pacific Oil and Gas Conference and Exhibition, OnePetro, 2005.

[54] A. Guleria, D. Swami, N. Joshi, A. Sharma, Application of temporal moments to interpret solute transport with time-dependent dispersion, Sādhanā 45 (1) (2020) 1–16.

[55] C. E. Divine, J. J. McDonnell, The future of applied tracers in hydrogeology, Hydrogeology journal 13 (1) (2005) 255–258.

[56] P. Somasundaran, L. Zhang, Adsorption of surfactants on minerals for wettability control in improved oil recovery processes, Journal of Petroleum Science and Engineering 52 (1-4) (2006) 198–212.

[57] G. M. Shook, G. A. Pope, K. Asakawa, Determining reservoir properties and flood performance from tracer test analysis, in: SPE Annual Technical Conference and Exhibition, Society of Petroleum Engineers, 2009.

[58] M. L. Brusseau, The influence of solute size, pore water velocity, and intraparticle porosity on solute dispersion and transport in soil, Water Resources Research 29 (4) (1993) 1071–1080.

[59] P. Ramachandran, M. Duduković, P. Mills, A new model for assessment of external liquid-solid contacting in trickle-bed reactors from tracer

response measurements, Chemical engineering science 41 (4) (1986) 855–860.

[60] L. Ferreira, F. Descant, M. Delshad, G. Pope, K. Sepehrnoori, A single-well tracer test to estimate wettability, in: SPE/DOE Enhanced Oil Recovery Symposium, Society of Petroleum Engineers, 1992.

[61] L. Baussaron, C. Julcour-Lebigue, A.-M. Wilhelm, C. Boyer, H. Delmas, Partial wetting in trickle bed reactors: measurement techniques and global wetting efficiency, Industrial & Engineering Chemistry Research 46 (25) (2007) 8397–8405.

[62] S. F. Shariatpanahi, S. Strand, T. Austad, Evaluation of water-based enhanced oil recovery (eor) by wettability alteration in a low-permeable fractured limestone oil reservoir, Energy & Fuels 24 (11) (2010) 5997–6008.

[63] K. P. Saripalli, H. Kim, P. S. C. Rao, M. D. Annable, Measurement of specific fluid- fluid interfacial areas of immiscible fluids in porous media, Environmental science & technology 31 (3) (1997) 932–936.

[64] K. P. Saripalli, P. Rao, M. Annable, Determination of specific napl–water interfacial areas of residual napls in porous media using the interfacial tracers technique, Journal of Contaminant Hydrology 30 (3-4) (1998) 375–391.

[65] M. Narter, M. L. Brusseau, Comparison of interfacial partitioning tracer test and high-resolution microtomography measurements of fluid-fluid interfacial areas for an ideal porous medium, Water resources research 46 (8) (2010).

[66] H. Zhong, A. El Ouni, D. Lin, B. Wang, M. L. Brusseau, The two-phase flow IPTT method for measurement of nonwetting-wetting liquid interfacial areas at higher nonwetting saturations in natural porous media, Water resources research 52 (7) (2016) 5506–5515.

[67] S. Strand, D. Standnes, T. Austad, New wettability test for chalk based on chromatographic separation of SCN^- and $SO4^{2-}$, Journal of Petroleum Science and Engineering 52 (1-4) (2006) 187–197.

[68] V. Jain, S. Bryant, M. Sharma, Influence of wettability and saturation on liquid- liquid interfacial area in porous media, Environmental science & technology 37 (3) (2003) 584–591.

[69] J. Schwartz, E. Weger, M. Duduković, A new tracer method for determination of liquid-solid contacting efficiency in trickle-bed reactors, AIChE Journal 22 (5) (1976) 894–904.

[70] Y. Lyu, M. L. Brusseau, W. Chen, N. Yan, X. Fu, X. Lin, Adsorption of pfoa at the air–water interface during transport in unsaturated porous media, Environmental science & technology 52 (14) (2018) 7745–7753.

[71] M. J. Blunt, Q. Lin, T. Akai, B. Bijeljic, A thermodynamically consistent characterization of wettability in porous media using high-resolution imaging, Journal of colloid and interface science 552 (2019) 59–65.

[72] A. Herring, C. Sun, R. Armstrong, Z. Li, J. McClure, M. Saadatfar, Evolution of bentheimer sandstone wettability during cyclic scco2-brine injections, Water Resources Research 57 (11) (2021) e2021WR030891.

[73] R. Huang, A. L. Herring, A. Sheppard, Effect of saturation and image resolution on representative elementary volume and topological quantification: An experimental study on bentheimer sandstone using micro-ct, Transport in Porous Media 137 (3) (2021) 489–518.

[74] G. Garfi, C. M. John, M. Rücker, Q. Lin, C. Spurin, S. Berg, S. Krevor, Determination of the spatial distribution of wetting in the pore networks of rocks, Journal of Colloid and Interface Science (2022).

[75] D. Singh, S. Roy, H. J. Pant, J. Phirani, Solid-fluid interfacial area measurement for wettability quantification in multiphase flow through porous media, Chemical Engineering Science 231 (2021) 116250.

[76] B. Zhao, C. W. MacMinn, R. Juanes, Wettability control on multiphase flow in patterned microfluidics, Proceedings of the National Academy of Sciences 113 (37) (2016) 10251–10256.

[77] J. H. Dane, C. G. Topp, Methods of soil analysis, Part 4: Physical methods, Vol. 20, John Wiley & Sons, 2020.

[78] J. Ding, Y. Zhang, S. Lu, X. Zhang, Y. Li, Y. Zhong, H. Zhang, A novel strategy using persulfate activated with thiosulfate for strong enhancement of trace 2, 2-dichlorobiphenyl removal: Influencing factors, and mechanisms, Chemical Engineering Journal 415 (2021) 128969.

[79] W. R. Paidin, Physical model study of the effects of wettability and fractures on gas assisted gravity drainage (gagd) performance (2006).

[80] N. Shahidzadeh-Bonn, A. Tournié, S. Bichon, P. Vié, S. Rodts, P. Faure, F. Bertrand, A. Azouni, Effect of wetting on the dynamics of drainage in porous media, Transport in porous media 56 (2) (2004) 209–224.

[81] M. Rezaveisi, S. Ayatollahi, B. Rostami, Experimental investigation of matrix wettability effects on water imbibition in fractured artificial porous media, Journal of Petroleum Science and Engineering 86 (2012) 165–171.

[82] M. A. Sohal, G. Thyne, E. G. Søgaard, Novel application of the flotation technique to measure the wettability changes by ionically modified water for improved oil recovery in carbonates, Energy & Fuels 30 (8) (2016) 6306–6320.

[83] A. E. Rodrigues, Residence time distribution (rtd) revisited, Chemical Engineering Science (2020) 116188.

[84] G. Findenegg, Principles of adsorption at solid surfaces and their significance in gas/solid and liquid/solid chromatography, in: Theoretical

Advancement in Chromatography and Related Separation Techniques, Springer, 1992, pp. 227–260.

[85] M. Omran, S. Akarri, O. Torsaeter, The effect of wettability and flow rate on oil displacement using polymer-coated silica nanoparticles: a microfluidic study, Processes 8 (8) (2020) 991.

[86] J. Stokes, D. Weitz, J. P. Gollub, A. Dougherty, M. Robbins, P. Chaikin, H. Lindsay, Interfacial stability of immiscible displacement in a porous medium, Physical review letters 57 (14) (1986) 1718.

[87] D. Quéré, Wetting and roughness, Annu. Rev. Mater. Res. 38 (2008) 71–99.

Highlights

- Measurement of solid-liquid interfacial area for multiphase flow in a porous medium.
- Water-solid interfacial area generally increases with increase in water saturation.
- Anomalous behaviour of the interfacial area for oil wet medium at residual saturations.
- Novel technique can be used for Darcy-scale quantification of wettability.

Jyoti Phirani: Conceptualization, Methodology, Supervision, Writing – Review & Editing, Funding acquisition, Project administration, Resources, Formal analysis

Deepshikha Singh: Investigation, Data curation, Writing – original draft, Software, Visualization, Formal analysis

Shantanu Roy: Methodology, Writing – Review & Editing, Funding acquisition

Harish J. Pant: Writing – Review & Editing, Resources,

Declaration of interests

☒ The authors declare that they have no known competing financial interests or personal relationships that could have appeared to influence the work reported in this paper.

☐ The authors declare the following financial interests/personal relationships which may be considered as potential competing interests: